

miRNA-490-3p promotes the metastatic progression of invasive ductal carcinoma

NING LU^{1*}, MEI ZHANG^{2*}, LU LU³, YAN-ZHAO LIU⁴, HAI-HONG ZHANG⁵ and XIAO-DONG LIU¹

¹Department of Breast Medical Oncology, Tianjin Medical University Cancer Institute and Hospital, National Clinical Research Center for Cancer, Key Laboratory of Cancer Prevention and Therapy, Tianjin's Clinical Research Center for Cancer, Key Laboratory of Breast Cancer Prevention and Therapy, Tianjin Medical University, Ministry of Education, Tianjin 300060;

²Department of Rheumatology and Immunology, Tianjin Medical University General Hospital, Tianjin 300052;

³Department of Pharmacy, Tianjin Medical University Cancer Institute and Hospital, National Clinical Research Center for Cancer, Key Laboratory of Cancer Prevention and Therapy, Tianjin's Clinical Research Center for Cancer, Tianjin 300060;

⁴Department of Medicine, Tianjin Medical University General Hospital, Tianjin 300052;

⁵Department of Human Resources, Tianjin Hospital, Tianjin 300211, P.R. China

Received June 3, 2020; Accepted November 10, 2020

DOI: 10.3892/or.2020.7880

Abstract. MicroRNA (miRNA/mir)-490-3p has been defined as a tumor suppressor in different types of cancer, including breast cancer. However, miR-490-3p has been shown to function as a tumor suppressor and promoter in a context-dependent manner in hepatocellular and lung cancer. Contrary to previous studies, the present study revealed that miR-490-3p expression was significantly higher in invasive ductal carcinoma (IDC) tissue specimens, the most common form of breast cancer, compared to tumor-adjacent normal tissue specimens (n=20). Its expression was also higher in the more metastatic breast cancer cell line, MDA-MB-231, compared to the non-metastatic breast cancer cell line, MCF7, and the moderately metastatic breast cancer cell line, MDA-MB-468. The expression of miR-490-3p was induced following transforming growth factor (TGF)- β -induced epithelial-to-mesenchymal transition (EMT) in MCF10A cells. Gain-and loss-of-function assays revealed that the expression of miR-490-3p regulated the proliferation, colony formation, EMT, migration and invasion *in vitro*, but not the apoptosis of MDA-MB-468 and MDA-MB-231 cells. The knockdown

of miR-490-3p expression in MDA-MB-231 cells inhibited experimental metastasis in a tumor xenograft assay. As in lung cancer, miR-490-3p was found to target and downregulate the expression of the tumor suppressor RNA binding protein poly r(C) binding protein 1 (PCBP1). PCBP1 protein and miR-490-3p expression inversely correlated in patients with ductal carcinoma *in situ* (DCIS; n=10; no nodal involvement) and IDC (n=10; different stages of metastatic progression) with a significantly higher miR-490-3p expression in patients with IDC compared to those with DCIS. The expression of miR-490-3p was negatively associated with both overall and disease-free survival in the patients with breast cancer included in the present study. On the whole, the results confirm a pro-metastatic role of miR-490-3p in IDC, establishing it as a biomarker for disease progression in these patients.

Introduction

Given the improvements made in diagnostics and mass awareness, and the development of novel treatment strategies, the incidence rate and mortality associated with cancer have decreased. However, breast cancer remains the major cause of cancer-associated mortality among women worldwide, with a progressive increase in its incidence rate (1,2). The majority of deaths due to breast cancer are due to resistance to chemotherapy and secondary progression (metastasis) to other organs (3-6). MicroRNAs (miRNAs or miRs) have been shown to be involved in different stages of carcinogenesis, either by targeting their cognate messenger RNA (mRNA) for degradation or effectively silencing translation of mRNA to the protein product (7,8).

miR-490-3p and miR-490-5p has been shown to function as tumor suppressors in colorectal cancer, renal cell carcinoma, epithelial ovarian cancer and bladder cancer (9-13). However, separate studies have demonstrated that miR-490-3p can function as a tumor suppressor or promoter in lung and hepatocellular carcinoma (14-17). miR-490-3p has also been

Correspondence to: Dr Ning Lu, Department of Breast Medical Oncology, Tianjin Medical University Cancer Institute and Hospital, National Clinical Research Center for Cancer, Key Laboratory of Cancer Prevention and Therapy, Tianjin's Clinical Research Center for Cancer, Key Laboratory of Breast Cancer Prevention and Therapy, Tianjin Medical University, Ministry of Education, Ti-Yuan-Bei, Huan-Hu-Xi Road, Hexi, Tianjin 300060, P.R. China
E-mail: tjmuchvip@163.com

*Contributed equally

Key words: poly r(C) binding protein 1, miR-490-3p, breast cancer, epithelial-to-mesenchymal transition, metastasis

shown to function as a tumor suppressor in breast cancer by targeting *RHOA*, which encodes Ras homolog gene family member A (18). However, it should be noted that in each of these studies, a different target of miR-490-3p has been identified. In the absence of RNAseq and functional data on the effects of miR-490-3p overexpression or knockdown, and the heterogeneity of the samples used in these studies, the true role of miR-490-3p in tumorigenesis is debatable.

Hence, the objective of the present study was to evaluate the role of miR-490-3p in breast cancer using a combination of *in vitro* cell lines with different metastatic potential and human breast cancer tissue specimens. The functional outcomes of the overexpression and knockdown of miR-490p-3p on cell proliferation and pro-invasive behavior were investigated. It was found that miR-490-3p, in contrary to the findings of a previous study (18), was overexpressed in human breast cancer tissue specimens and exhibited pro-metastatic behavior in breast cancer cell lines. In addition, the present study revealed that as in lung cancer (16), the pro-metastatic behavior of miR-490-3p in breast cancer was mediated by targeting the tumor suppressor poly r(C) binding protein 1 (PCBPI).

Materials and methods

Human tissue samples. All human studies were conducted in accordance with a protocol approved by the Institutional Review Board of the Tianjin Medical University Cancer Institute and Hospital. Human breast cancer and tumor adjacent normal tissues were obtained from 45 female patients [35 patients with invasive ductal carcinoma (IDC) and 10 patients with ductal carcinoma *in situ* (DCIS) sub-types] at the Tianjin Medical University Cancer Institute and Hospital. Tissue specimens were not included from patients that had undergone prior chemotherapy. All enrolled patients provided written consent and were followed-up for up to 150 months. Tissue specimens were either processed immediately after acquiring or were stored in liquid nitrogen for future use. The clinicopathological characteristics of the included patients are detailed in Table SI.

Cell lines. The normal breast epithelial cell line, MCF10A (CRL10317) (19), and the breast cancer cell lines, MCF7 (HTB-22), MDA-MB-468 (HTB-132) and MDA-MB-231 (HTB-26) (20,21), were obtained from the American Type Culture Collection (ATCC). MCF10A cells were cultured in DMEM/F12 media supplemented with horse serum (5%), EGF (20 ng/ml), hydrocortisone (250 µg/ml), cholera toxin (100 ng/ml) and insulin (0.1 mg/ml), whereas the other cell lines were cultured in DMEM containing 10% fetal bovine serum. For transforming growth factor (TGF)-β stimulation, the cells were stimulated with TGF-β at 5 ng/ml for 3 days.

Isolation of RNA, miRNA and detection by RT-qPCR. RNA was isolated using TRIzol reagent (Thermo Fisher Scientific, Inc.) based on the manufacturer's protocol. The PureLink miRNA isolation kit (Thermo Fisher Scientific, Inc.) was used for miRNA isolation. TaqMan probes were used for the RT-qPCR detection of *PCBPI*, *TBP*, hsa-miR-490-3p and *RNU6B* (assay ID: Hs00362410_s1, Hs00427620_m1, 001037

and 001093, respectively; Thermo Fisher Scientific, Inc.). Each cDNA sample was pre-amplified using the TaqMan PreAmp Master Mix kit (Thermo Fisher Scientific, Inc.) and then used to template the qPCR using the TaqMan Fast Advanced Master Mix and TaqMan mRNA or miRNA assay probes. The thermocycling conditions consisted of an initial denaturation of 20 sec at 95°C, followed by 40 cycles of 95°C for 3 sec and 60°C for 30 sec. Raw threshold values were normalized to *TBP* and *RNU6B* expression for *PCBPI* and *hsa-miR-490-3p*, respectively, and the data were then analyzed using the standard $2^{-\Delta\Delta C_q}$ method (22).

Overexpression and reporter plasmids. *miR-490-3p* was cloned as previously described (14). *PCBPI* 3'UTR luciferase and control pGL3 constructs were purchased from Promega Corporation. The miR-490-3p seed region mutant of the *PCBPI* 3'UTR was made by site-directed mutagenesis by deleting nucleotides 77-83, that corresponded to the complementary region of the seed sequence of miR-490-3p. The prediction of the miR-490-3p binding site was performed using TargetScan v7.1 (http://www.targetscan.org/vert_71/).

Transient transfection and luciferase assay. Lipofectamine LTX along with the PLUS reagent (Thermo Fisher Scientific, Inc.) were used for all transient transfactions entirely based on the manufacturer's provided protocol. Transfection was performed in a 24-well plate and cells were transfected with 0.25 µg each of *PCBPI* 3'UTR wild-type or mutant *Renilla* luciferase and pGL3 Firefly luciferase (control) plasmids. Where indicated, cells were transfected with pcDNA3 or pcDNA3/pri-miR-490-3p (Origene) (0.25 µg) and 30 nM of control or miR-490-3p antisense oligos (ASOs; Thermo Fisher Scientific, Inc.) using Lipofectamine LTX along with the PLUS reagent at 72 h prior to the transfection of the luciferase plasmids. Luciferase assay was performed at 48 h following transfection using the Dual Luciferase Assay kit from Promega Corporation. *Renilla* luciferase values were normalized to Firefly luciferase values and the relative *Renilla*/Firefly luciferase (relative fluorescent units) were plotted.

5-Bromo-2'-deoxyuridine (BrdU) labeling: Cell proliferation assay. Cell proliferation was assessed using the BrdU labeling kit (cat. no. B23151; Thermo Fisher Scientific, Inc.). BrdU labeling was performed for 2 h and the cells were then permeabilized using Triton X-100 based buffer. Cells were imaged using fluorescence microscope and number of fluorescent labeled cells in 3 random fields were determined to calculate percent labeled cells. Percentages of labeled cells were calculated from experiments performed in triplicate and plotted as the means ± standard deviation (SD).

Colony formation assay. MDA-MB-468 cells (transfected with pcDNA3 or pcDNA3/pri-miR-490-3p) and MDA-MB-231 (transfected with scrambled control or miR-490-3p ASO cells were suspended in complete medium containing low-melting agarose (0.35% v/v). Cells (1.0x10³/well) were plated on 0.6% solidified agarose in complete medium in 6-well plates. Cells were fixed with 10% formalin for 10 min after 3 weeks. The fixed cells were stained with 0.05% crystal violet dye (Sigma-Aldrich; Merck KGaA) for 15 min at room temperature and excess stain

was washed with phosphate-buffered saline (PBS). Cell colony numbers were imaged using a Scienceware colony counter system (Sigma-Aldrich; Merck KGaA; cat. no. Z378518) and counted in 5 different fields.

Annexin V/PI staining: Apoptosis assay. Cells were labeled with Annexin V/PI (BD Biosciences) based on the supplied protocol. Flow cytometry-based detection was performed for Annexin V and PI using a LSRFortessa Flow Cytometer (BD Biosciences; cat. no. 649225). Data were analyzed using BD FACSDiva Software v9.0 (BD Biosciences). Annexin V⁺/PI⁻ cells were considered to be early apoptotic. Annexin V⁺/PI⁺ cells were considered to be late apoptotic. The percentages early and late apoptotic cells determined from 3 independent experiments are presented as the means ± SD.

Western blot analysis. At the end of the indicated treatments, the cells were rinsed with ice-cold PBC and then lysed with RIPA lysis buffer. Protein concentrations were determined using the BCA protein assay kit (Thermo Fisher Scientific). Proteins (50 µg) were run on 10% SDS-PAGE gels and transferred to PVDF membranes. Membranes were blocked using 5% fat-free milk for 1 h at room temperature. Antibodies used to probe the blots were Vimentin (ab24525), EpCAM (ab71916), PCBP1 (ab171681), E-Cadherin (ab76055), GATA3 (ab106625), cyclin D1 (ab16663), cyclin E (ab71535), CDK2 (ab232753), CDK4 (ab226474), CDK6 (ab84717) and TBP (ab28175) (all from Abcam). All antibodies were used at a 1:1,000 dilution. Blots were incubated with the primary antibodies overnight at 4°C. Blots were probed with TBP to confirm that equivalent amounts of proteins were loaded in each case. Post-incubation with primary antibodies, blots were washed thrice with 1X PBS and then incubated with goat anti-mouse IgG H&L (HRP) (ab6789; Abcam) or goat anti-rabbit IgG1 IgG H&L (HRP) (ab6721; Abcam) secondary antibody at 1:5,000 dilution for 1 h at room temperature. Post-incubation blots were washed thrice with 1X PBS. Blots were visualized using ECL Plus kit (Thermo Fisher Scientific, Inc.) and HyBlot CL film (Denville Scientific).

In vitro pro-metastatic (migration and invasion) assays. All migration and invasion assays were performed using Cultrex 96-well inserts (R&D Systems, Inc.) according to the manufacturer's protocols. Basement membrane extract (BME) was used to coat the wells for the invasion assays. For both migration and invasion assays, serum-starved (starved for 16 h) cells (5×10^4 /well) were seeded in the top wells and normal medium was used as the chemoattractant in the bottom wells. After 18 h of incubation in 5% CO₂ and at 37°C, the migrating or invading cells were determined using Calcein-AM containing cell dissociation buffer. Readings were obtained at a 485 nm excitation and 520 nm emission using SPARK MicroPlate Reader (Group, Ltd.). Relative fluorescent units were converted to cell numbers using standard curves. The percentage migration and invasion were calculated as [(no. of migrating or invading cells x100)/50,000)].

Tissue microarray (TMA) analysis. The TMAs were generated from tumor tissue specimens obtained from patients diagnosed with DCIS (n=10) and IDC (n=10). Slides were stained with anti-PCBP1 (ab171681; Abcam; 1:125 dilution) based on

previously reported protocols (23,24). Incubation with primary antibody was done overnight at 4°C. Blinded evaluation and staining score (intensity score of 0-3 and percentage staining score of 0-5, which were combined to obtain a total staining score) were performed by a pathologist.

Immunofluorescence staining. Immunofluorescence staining for vimentin was performed using anti-Vimentin antibody (ab24525; Abcam) at a 1:50 dilution (overnight incubation at 4°C). The excess antibody was washed off using 3 washes of 15 min each with 1X PBS and the cover slips were then incubated with cy3-goat anti-rabbit IgG secondary antibody (ab6939, Abcam) (1:50) and 20 µl anti-fluorescence attenuation sealer for 1 h at room temperature. The coverslips were then mounted using VECTASHIELD Antifade containing 4,6-diamidino-2-phenylindole (DAPI; Vector Laboratories, Inc.). Images were obtained using a Zeiss LSM 510 META confocal laser scanning microscope (Carl Zeiss Microscopy LLC).

Data mining. The Cancer Genome Atlas (TCGA) data analyses were performed using cBioPortal for Cancer Genomics (<http://cbioportal.org>) (25,26). This included 7,084 patients with >7,251 samples from 12 studies. The analysis was performed to determine genetic alterations.

Tumor xenograft assay. All animal experiments were approved by the Institutional Animal Care and Use Committee of the Tianjin Medical University Cancer Institute and Hospital. MDA-MB-231 cells were transduced with a Firefly luciferase expression lentivirus and selected for 2 weeks using puromycin (2 µg/ml). Athymic nude mice (The Jackson Laboratory) were maintained in a pathogen-free environment at room temperature with 12-h light/dark cycle and free access to food and water. Mice (6 weeks old; weighing approximately 20 g) were injected via the tail vein with 1×10^6 MDA-MB-231 cells (n=8). The animals were randomly divided into 2 groups (n=4 per group). Mice were administered with either the control or miR-490-3p ASO (4 mg/kg body weight) via tail vein every alternate day, commencing on day 0. Animals were imaged using IVIS Spectrum In Vivo Imaging System (PerkinElmer, Inc.; cat. no. 124262) every 7 days following an intraperitoneal injection of D-luciferin (Xenogen; 150 mg/kg in 200 µl). The mice were euthanized at 21 days after injection, and the lungs were harvested and stored in formalin. Tissue specimens were processed and were used for H&E staining or immunohistochemistry (IHC) using routine methodologies. Briefly, paraffin-embedded blocks were sectioned at 5 µm thickness using a microtome (Model HM310, Microm Inc.), dewaxed with xylene, and cleared with a series of changing ethanol concentrations. Blocking was performed by incubation in 5% bovine serum albumin (Thermo Fisher Scientific, Inc.) and 0.3% Triton-X-100 (Thermo Fisher Scientific, Inc.) for 1 h at room temperature. Slides were incubated with anti-N-cadherin antibody (Clone EPR1791-4; ab76011) (1:250 dilution in 5% BSA; Abcam) overnight at 4°C. Post-incubation excess stained was washed off by 3 rinses with 1X PBS and then incubated with horseradish peroxidase-conjugated anti-rabbit secondary antibody (1662408EDU; Bio-Rad Laboratories, Inc.; 1:3,000 dilution in 5% BSA) for 1 h at room temperature. Following washing thrice with PBS, slides were developed

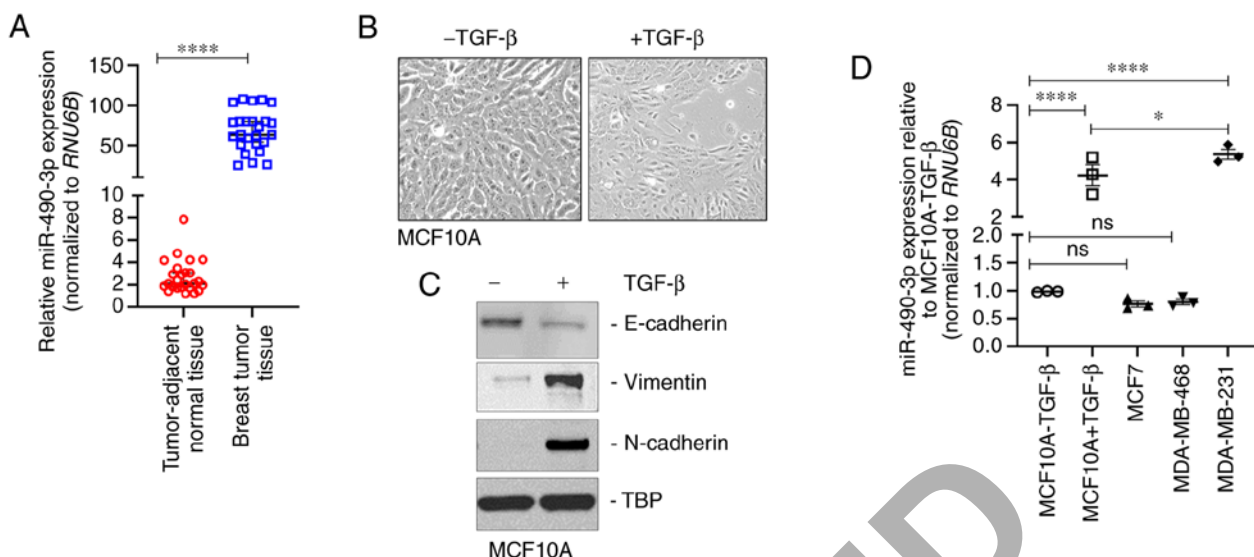


Figure 1. *miR-490-3p* expression is positively associated with metastatic breast cancer. (A) Steady-state expression of *miR-490-3p* in paired tumor and tumor-adjacent normal breast tissue specimens from 25 female patients with invasive ductal carcinoma. Data were normalized to *RNU6B* expression. Error bars represent the median with 95% CI. ***P<0.0001. (B and C) TGF- β stimulation of MCF10A cells for 3 days induced EMT. Shown are (B) representative photo micrographs and western blots of epithelial and mesenchymal cell markers (C). TBP was used as a loading control in (C). (D) Steady-state expression of *miR-490-3p* in MCF10A ± TGF- β , MDA-MB-468, MCF7 and MDA-MB-231 cells. Data were normalized to *RNU6B* expression and are expressed relative to MCF10A-TGF- β . Error bars represent the mean \pm SEM; *P<0.05, ***P<0.0001; ns, not significant (P>0.05). EMT, epithelial-mesenchymal transition.

with DAB (Abcam). Slides were viewed by imaging using a Color View II; Soft Imaging System (Olympus Optical GmbH).

Statistical analyses. Statistical analysis was carried out using SPSS 20.0 software (IBM Corporation). The distribution of the data was determined using the Shapiro-Wilk test. Continuous variables are presented as the means \pm standard deviation. The comparison of *miR-490-3p* expression between breast tumor tissues compared to tumor-adjacent normal tissues was performed using a paired Student's t-test. Statistical significance between groups was calculated using one-way ANOVA with Tukey's post hoc test. P<0.05 was considered to indicate a statistically significant difference. The correlation between PCBP1 and *miR-490-3p* was calculated by the Spearman's rank correlation test. Kaplan-Meier curves were computed to analyze survival rates and the log-rank (Mantel-Cox) test was used to evaluate statistical significance.

Results

***miR-490-3p* is overexpressed in human breast cancer and pro-metastatic breast cancer cell lines.** *miR-490-3p* expression was determined in breast tumor and tumor-adjacent normal tissue specimens from 25 female patients with IDC. All patients exhibited metastatic progression and either had stage IIIB or IV disease. *miR-490-3p* expression was significantly higher in the breast tumor tissues compared to tumor-adjacent normal tissues (Fig. 1A). In order to determine alterations in the expression of *miR-490-3p* during metastasis, changes in expression changes were initially determined in cells undergoing epithelial-to-mesenchymal transition (EMT), an important pre-requisite for metastatic progression (27,28). The present study used the non-transformed breast epithelial cell line, MCF10A, as a model, and the cells underwent EMT when stimulated with TGF- β treatment for 3 days. Epithelial MCF10A cells are cuboid-shaped and

tightly packed; however, following stimulation with TGF- β for 3 days, the cells became spindle-shaped, mimicking the phenotypic characteristics of mesenchymal cells (Fig. 1B). Western blot analysis revealed the decreased expression of the epithelial cell marker, E-cadherin, and the increased expression of the mesenchymal cell markers, vimentin and N-cadherin (Fig. 1C) following TGF- β stimulation, confirming the observed phenotypic changes (Fig. 1B). *miR-490-3p* expression was significantly higher in the mesenchymal MCF10A (TGF- β -stimulated) cells in comparison to the untreated epithelial MCF10A cells (Fig. 1D). In addition, *miR-490-3p* expression was assessed in the MCF7 (non-metastatic breast cancer cell line), MDA-MB-468 (moderately metastatic triple negative breast cancer cell line) and MDA-MB-231 (highly metastatic breast cancer cell line) cells. Compared with the epithelial MCF10A cells, the expression of *miR-490-3p* was significantly higher in the MD-MB-231 cells, but not in the MCF7 or MDA-MB-468 cells (Fig. 1D). These results indicated that *miR-490-3p* expression was associated with the metastatic progression of breast cancer.

***miR-490-3p* expression affects the proliferation, but not the apoptosis of breast cancer cell lines.** The present study then determined whether the expression of *miR-490-3p* affects the proliferation and apoptosis of breast cancer cell lines. The MDA-MB-468 cells, which exhibited a lower *miR-490-3p* expression than the MDA-MB-231 cells (Fig. 1D), were transfected with *miR-490-3p* overexpression or control plasmid. By contrast, the MDA-MB-231 cells, which exhibited a relatively higher expression of *miR-490-3p* in comparison to the MDA-MB-468 cells (Fig. 1D), were transfected with *miR-490-3p* or control ASO. The relative expression of *miR-490-3p* post-transfection in these cell lines was confirmed by RT-qPCR (Fig. 2A). Cell proliferation was determined at 72 h post-transfection using BrdU labeling. The overexpression of *miR-490-3p* significantly increased the proliferation

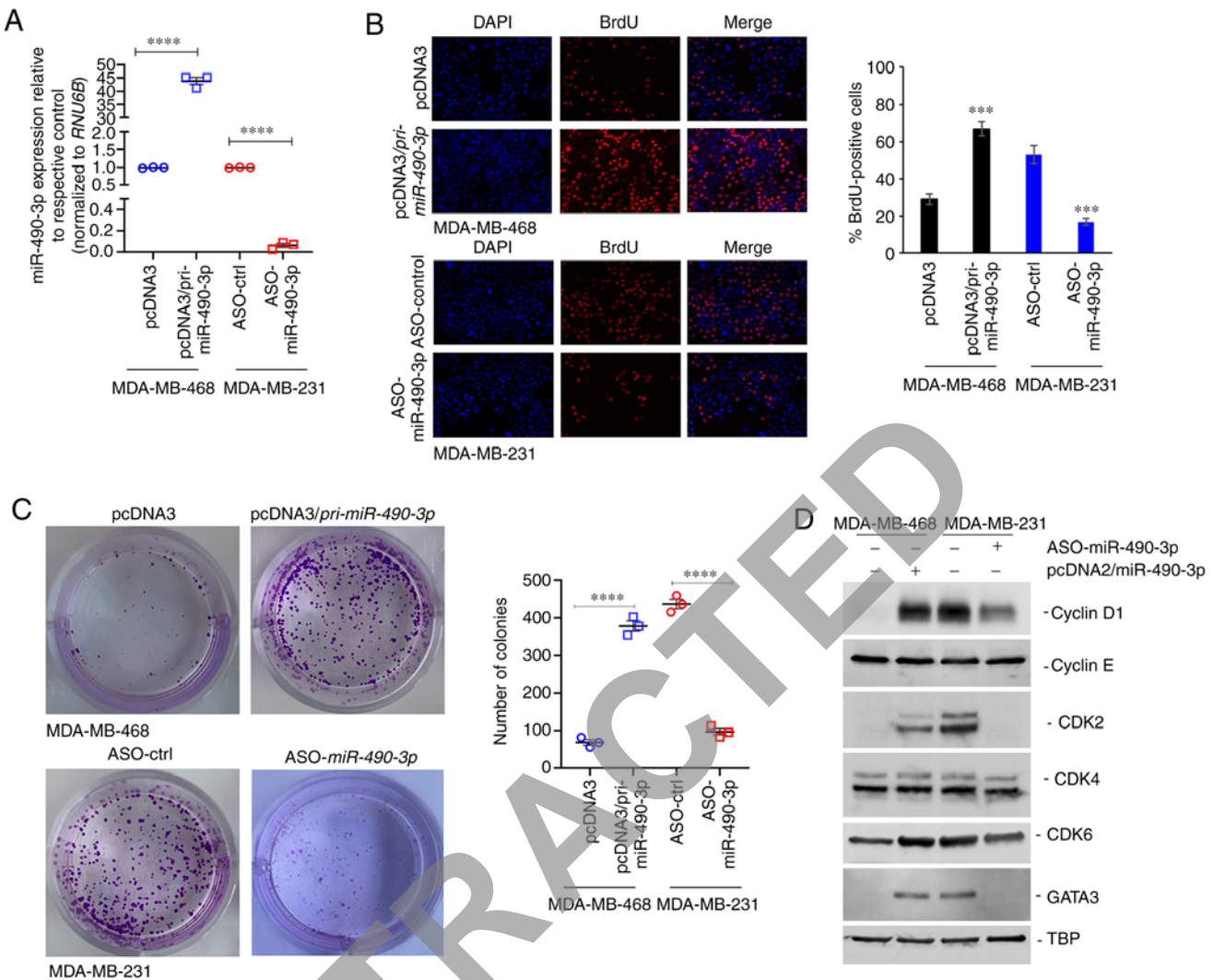


Figure 2. *miR-490-3p* expression levels regulate the proliferation of breast cancer cells *in vitro*. (A) Successful overexpression and inhibition of *miR-490-3p* in MDA-MB-468 and MDA-MB-231 cells, respectively, as confirmed by RT-qPCR. Data were normalized to *RNU6B* and are expressed relative to the controls (pcDNA3 for MDA-MB-468 and ASO-ctrl for MDA-MB-231). (B) Cell proliferation was measured in indicated cells 72 h following transfection by BrdU labeling. (C) Colony formation by indicated cells was determined by soft agar assay. Shown are relative number of colonies after 3 weeks. (D) Representative western blots of different regulators of cell cycle progression in the indicated cells. TBP was used as a loading control. (A-C) Error bars represent the mean \pm SD; ***P<0.001, ****P<0.0001.

of the MDA-MB-468 cells, whereas the use of ASO in the MDA-MB-231 cells significantly decreased cell proliferation (Fig. 2B). The effect on cell proliferation was mimicked in colony formation assays. The ectopic expression of *miR-490-3p* significantly increased the number of colonies in the MDA-MB-468 cells, whereas the knockdown of endogenous *miR-490-3p* using ASO significantly decreased the number of colonies in the MDA-MB-231 cells (Fig. 2C). Given the observed increase in cell proliferation and soft agar growth, the expression of cell cycle regulatory proteins was then investigated in these cells. The ectopic expression of *miR-490-3p* induced the expression of cyclin D1, CDK2, CDK6 and GATA3, but not that of cyclin E and CDK4 in the MDA-MB-468 cells. The knockdown of endogenous *miR-490-3p* using ASO in the MDA-MB-231 resulted in the decreased expression of cyclin D1, CDK2, CDK6 and GATA3, whereas it had no effect on CDK4 and cyclin E expression (Fig. 2D). Taken together, these results indicate that *miR-490-3p* regulates the G1/S transition, potentially via the GATA3/cyclin D1 axis.

However, the expression of *miR-490-3p* did not have any effect on the apoptosis of either the MDA-MB-231 or MDA-MB-468 cells, as determined by Annexin V/PI staining (Fig. 3A and B), indicating a role of *miR-490-3p* expression levels in cell growth by driving cell proliferation.

miR-490-3p expression affects the pro-metastatic functions (migration and invasion) of breast cancer cell lines *in vitro*. One of the important properties of metastatic cancer cells is their ability to invade through the extracellular matrix and migrate to a secondary site. Hence, the present study then investigated whether modulating the expression of *miR-490-3p* in the cells would affect their ability to migrate and invade *in vitro*. The overexpression of *miR-490-3p* in the MDA-MB-468 cells significantly increased their migration and invasion *in vitro*; however, *miR-490-3p* ASO significantly decreased the migration and invasion of the MDA-MB-231 cells (Fig. 3C). These results indicated that expression of *miR-490-3p* was associated with an increased cell proliferation and an enhanced ability to migrate/invoke.

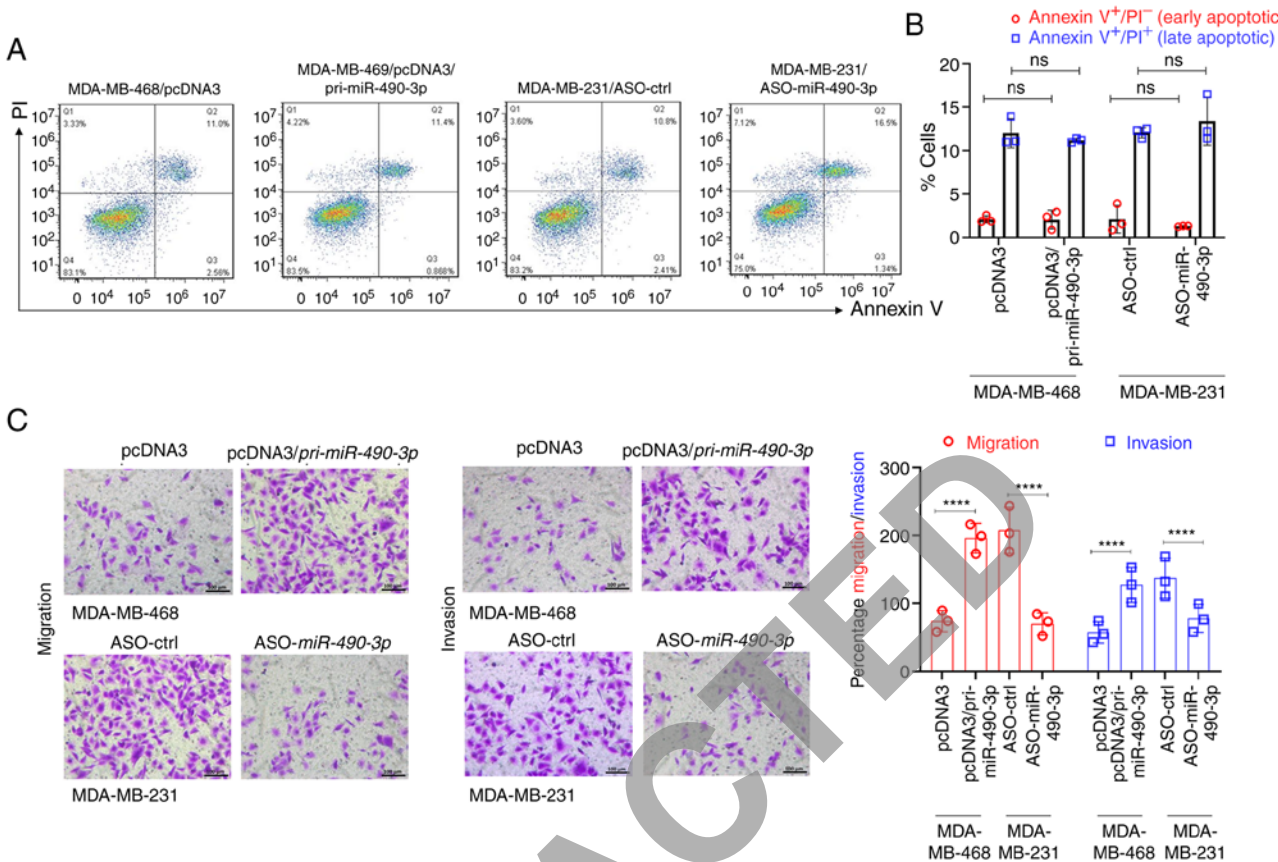


Figure 3. *miR-490-3p* expression levels do not affect apoptosis, but regulate the migration and invasion of breast cancer cells *in vitro*. (A and B) Apoptosis was measured in the indicated cells 72 h following transfection by Annexin V/PI staining. Shown are (A) representative flow cytometry dot plots and (B) quantification of early (Annexin V⁺/PI⁻) and late apoptotic (Annexin V⁺/PI⁺) cells. (C) Modulation of *miR-490-3p* affected cell migration and invasion. The migrated and invasive cells were imaged under a microscope, and the number of the migrated and invasive cells in each field was counted and represented as percent of total cells at the beginning of the assay. Error bars represent the mean \pm SD; ***P<0.0001; ns, not significant (P>0.05).

miR-490-3p expression affects the EMT and metastatic progression of breast cancer cells. Since EMT is an important pre-requisite for cancer cells to migrate and invade (26-28), the present study then investigated whether the *miR-490-3p* expression levels were associated with the ability of the cells to undergo EMT. Increasing the overexpression of *miR-490-3p* in the MDA-MB-468 cells decreased the expression of the epithelial cell markers, E-Cadherin and EpCAM, and increased expression of the mesenchymal cell markers, Vimentin and N-Cadherin (Fig. 4A and B). Conversely, *miR-490-3p* ASO increased the expression of E-Cadherin and EpCAM, and decreased the expression of Vimentin and N-Cadherin in the MDA-MB-231 cells (Fig. 4A). These results provided evidence that the *miR-490-3p* expression levels were connected to the phenotypic (Fig. 4) and functional (Fig. 3C) properties associated with the metastatic progression of breast cancer cells.

To determine whether the results obtained *in vitro* were applicable in an *in vivo* model of experimental breast cancer metastasis, tumor xenograft assays were performed using mice via tail vein injection. MDA-MB-231 cells expressing Firefly luciferase were injected via the tail vein into athymic nude mice. Injected mice were injected on alternate days with control or *miR-490-3p* ASO. Mice were imaged for up to 3 weeks after which lung tissue was harvested and processed for H&E and IHC staining. The mice injected with

the MDA-MB-231 cells expressing control ASO exhibited lung metastasis after 3 weeks (Fig. 4C), mice injected with MDA-MB-231 cells expressing *miR-490-3p* ASO exhibited an almost complete attenuation of lung colonization (Fig. 4D). H&E staining confirmed the presence of more metastatic colonies in the lungs of mice injected with cells expressing control ASO compared to the lungs of mice injected with cells expressing *miR-490-3p* ASO (Fig. 4E). To confirm that the cells resulting in lung colonization were the breast cancer cells and that this was not due to the high-pressure tail vein injection, IHC analysis was performed for the mesenchymal cell marker, N-cadherin. Lungs obtained from mice injected with control ASO exhibited a robust expression of N-cadherin in comparison to the low expression of N-cadherin in lungs obtained from mice injected with *miR-490-3p* ASO (Fig. 4F). Cumulatively, these results proved that *miR-490-3p* expression was associated with experimental metastasis *in vivo*.

miR-490-3p targets *PCBP1* in human breast cancer. It has been previously demonstrated that the RNA binding protein, *PCBP1*, is a direct target of *miR-490-3p* in lung cancer (16). Given the known role of *PCBP1* as a tumor suppressor in breast cancer (26,28), the present study then evaluated whether *PCBP1* was a target of *miR-490-3p* in breast cancer. It was initially confirmed using TargetScan that the 3'UTR of *PCBP1* indeed has a sequence complementary to the seed sequence

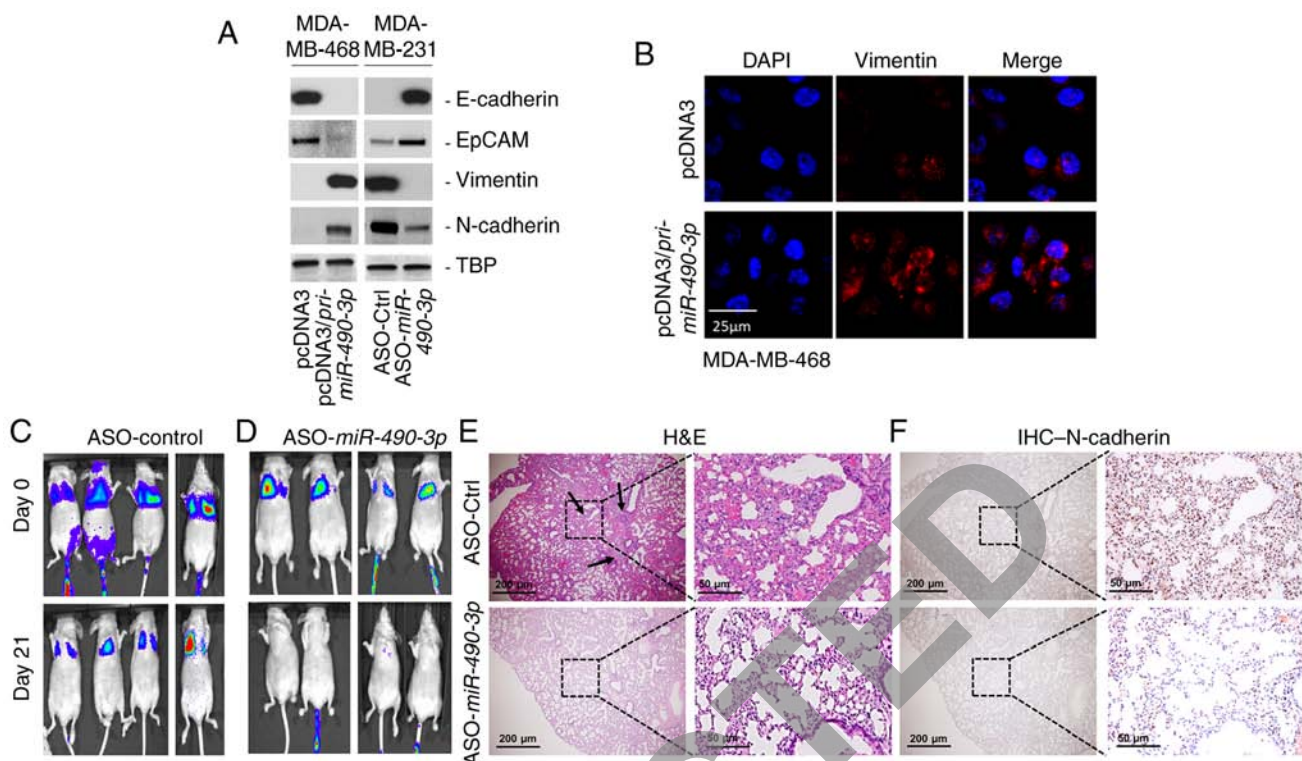


Figure 4. *miR-490-3p* expression levels drive EMT *in vitro* and experimental metastasis in breast cancer cell lines *in vivo*. (A) Western blot analysis of epithelial (E-cadherin and EpCAM) and mesenchymal (N-cadherin and vimentin) cell markers in indicated cells. TBP was used as a loading control. (B) Immunofluorescence analysis of vimentin in MDA-MB-468 cells transfected with control pcDNA3 or pcDNA3/ *miR-490-3p* plasmid. (C and D) Live *in vivo* luciferase imaging of mice injected with MDA-MB-231 cells and administered with (C) control ASO and (D) *miR-490-3p* ASO on days 0 and 21 post-injection. Luciferase signal in lungs is indicative of lung colonization. (E) Lungs from both experimental groups were harvested following the humane euthanasia of the mice in both experimental groups and processed for H&E staining. Arrows indicate macrometastatic lesions. (F) Lungs specimens excised from both experimental groups were probed for the pro-metastatic factor N-cadherin to confirm that the lesions observed are indeed metastatic and arise from the breast cancer cells. Magnified images are shown on the right for indicated areas shown on the left.

of *miR-490-3p* (Fig. 5A). Luciferase reporter assays were then performed to determine whether *PCBP1* was indeed a target of *miR-490-3p* in breast cancer cells. Relative luciferase reporter expression was significantly higher in the MDA-MB-468 cells compared to the MDA-MB-231 cells (Fig. 5B); *PCBP1* expression was inversely associated with the expression level of *miR-490-3p* in these cells (Fig. 1D). However, when the *miR-490-3p* binding site was deleted in the reporter plasmid, there was no marked difference in relative reporter expression between the MDA-MB-231 and MDA-MB-468 cells (Fig. 5B), indicating that *miR-490-3p* was targeting *PCBP1* in these cells. Further confirmation of *miR-490-3p* targeting *PCBP1* in these cells was provided from reporter assays following the transient transfection of pcDNA3/pri-miR-490-3p plasmid and *miR-490-3p* ASO into MDA-MB-468 and MDA-MB-231 cells, respectively. Reporter expression in the MDA-MB-231 cells was rescued following transfection with *miR-490-3p* ASO, whereas reporter expression was suppressed in the MDA-MB-468 cells transfected with the pcDNA3/pri-miR-490-3p plasmid (Fig. 5C). Western blot analysis of *PCBP1* in the MDA-MB-468 and MDA-MB-231 cells, parental or transfected with *miR-490-3p* plasmid and ASO, respectively mimicked the changes observed in relative reporter expression (Fig. 5D), confirming the *miR-490-3p*-mediated targeting of *PCBP1* in these cells.

Expression of PCBP1 and miR-490-3p inversely correlates with human breast cancer and is associated with disease

progression. RT-qPCR for *miR-490-3p* was performed in 20 human breast cancer and tumor-adjacent normal tumor samples (DCIS, n=10; and IDC, n=10). The expression of *miR-490-3p* was significantly lower in all 10 patients with DCIS compared to the 10 patients with IDC. The patients with DCIS had no nodal involvement, whereas all the IDC cases had some degree of metastatic progression, confirming the findings obtained above in that *miR-490-3p* expression is associated with metastatic progression. These 20 cases were further processed for *PCBP1* expression by IHC. A robust *PCBP1* expression was observed in cancer cells within the DCIS samples, whereas a low and scattered *PCBP1* expression was observed in cancer and stromal cells in the IDC samples (Fig. 6B and C). The relative *miR-490-3p* expression in the DCIS and IDC samples was then plotted with the corresponding IHC score for *PCBP1* expression. *PCBP1* and *miR-490-3p* expression inversely correlated (Fig. 6A; Spearman's correlation coefficient, R=-0.801; P<0.05).

Given the current observations, the TCGA dataset on breast cancer samples was then analyzed to identify genomic alterations in *miR-490/3P* in 7,084 patients across 7,251 samples from 12 studies (Fig. S1) (25,26,29). Isolated cases of genomic amplifications and deep deletions were identified (Fig. S2); however, the overall rate of genetic alterations was largely insignificant occurring in only 4.2% patients in one of the 12 studies.

Subsequently, the present study determined whether the overall survival (OS) and disease-free survival (DFS)

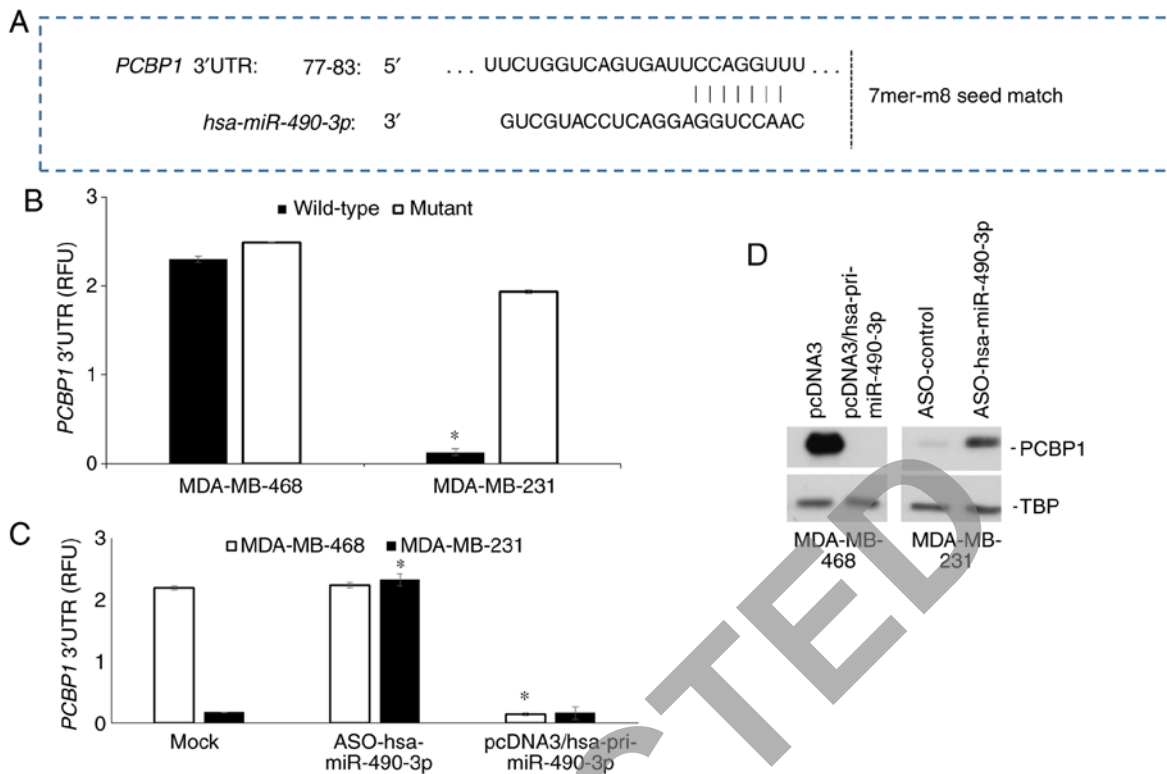


Figure 5. *PCBP1* is a target of *miR-490-3p* in breast cancer cells. (A) Complementary 7mer-m8 seed match between *miR-490-3p* and the 3'UTR of *PCBP1* as predicted by TargetScan software. (B) Relative luciferase activity of transiently transfected luciferase reporter constructs containing either full-length or mutated (*miR-490-3p* binding site deleted) *PCBP1* 3'UTR in indicated cells. *P<0.05. Error bars represent the mean ± SD. (C) Relative luciferase activity of transiently transfected luciferase reporter constructs containing full-length *PCBP1* 3'UTR in indicated cells, alone or in combination with *miR-490-3p* mimic and antagomir. *P<0.05 compared to respective mock control. Error bars represent the mean ± SD. (D) Western blot analysis of *PCBP1* in MDA-MB-468 and MDA-MB-231 cell lines transfected with *miR-490-3p* antagomir and mimic, respectively. TBP was used as a loading control.

of the 45 patients with breast cancer (35 patients with IDC and 10 patients with DCIS) included in the present study was associated with *miR-490/3P* expression level. The OS was significantly lower in patients with IDC (higher *miR-490-3p* expression) compared to patients with DCIS (lower *miR-490-3p* expression) [hazard ratio (HR), 5.466; 95% CI, 1.767-16.91] (Fig. 7A). Similarly, DFS was significantly higher in patients with DCIS compared to patients with IDC (HR, 8.799; 2.702-28.66) (Fig. 7B). Taken together, these results indicated that the expression of *miR-490-3p* was associated with a poor prognosis and lower OS.

Discussion

The results of the present study consistently revealed a higher expression of *miR-490-3p* in patients with IDC compared to patients with DCIS, and its expression was inversely associated with OS and DFS. These results are in apparent contradiction with those of a previous study indicating that *miR-490-3p* functions as a tumor suppressor in breast cancer (18). Zhao and Zheng (2016) evaluated *miR-490-3p* in paired specimens from 137 cases with invasive breast cancer (18). However, the disease stage or nodal involvement were not mentioned. In comparison, 34/35 patients with IDC patients in the present study were ≥N2 and none of the patients with DCIS had any nodal involvement. It was thus hypothesized that the apparent difference in the findings between the present study and the previously reported one (18) may be due to the difference in the degree of metastatic disease

progression (nodal involvement) of the patients enrolled in the two studies. The present results, *in vitro*, *in vivo* and in human patient samples clearly indicate that *miR-490-3p* expression is associated with metastatic progression. The results confirm that the *miR-490-3p* expression level varies and increases with disease progression. However, future studies are definitely required on a broader and more heterogenous sample sets of breast cancer subtypes to more accurately define the correlation of *miR-490-3p* expression with grade, stage, molecular sub-types and metastatic disease state.

miR-490 functions as a tumor suppressor in epithelial ovarian cancer, colorectal cancer, renal cell carcinoma and bladder cancer (8-12). Even within the context of hepatocellular and lung carcinoma, the association of *miR-490-3p* expression with disease progression seems to be context-dependent (13-16).

Another interesting aspect is that different studies have identified different targets of *miR-490-3p*, including *ERGIC3*, *CDK1*, *ATG7*, *VDAC1*, *PIK3CA*, *CCND1* and *PCBP1* (8-18). The present study solely focused on *PCBP1*, as it has been shown to be targeted by *miR-490-3p* (16) and due to its well-documented role as a tumor suppressor in breast cancer (23,24). Indeed, *PCBP1* has been shown to function as a tumor suppressor in different types of cancers (30-38) and it remains to be determined whether *miR-490-3p* regulates *PCBP1* expression in all those tumors. Furthermore, the function of *PCBP1* in breast cancer is regulated at the post-translational stage (23,24) and it remains to be determined whether *miR-490-3p* is a redundant

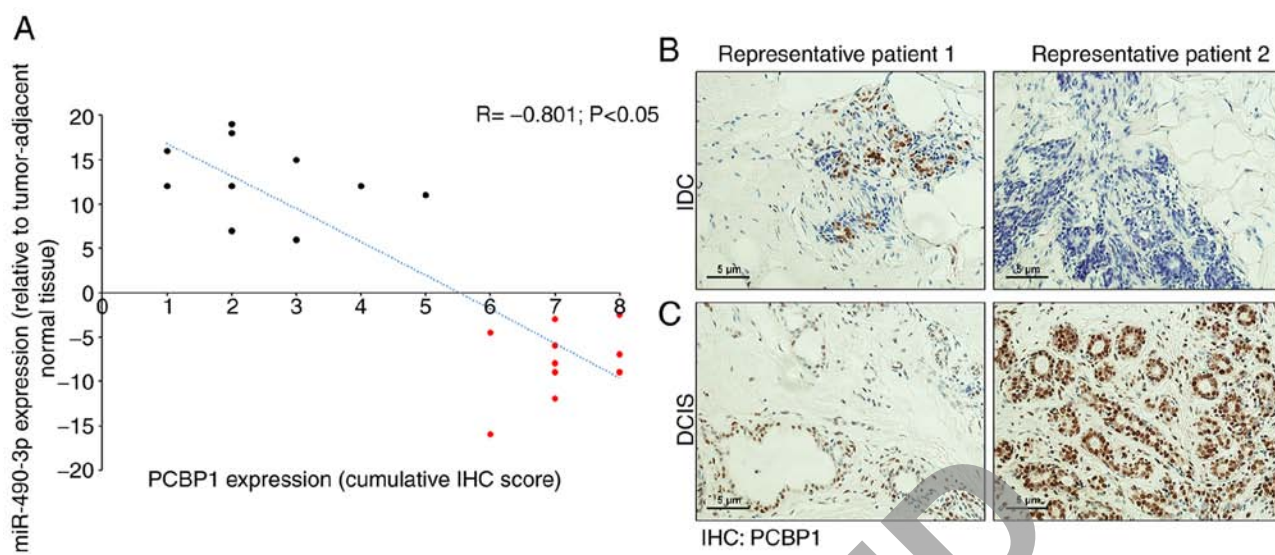


Figure 6. *miR-490-3p* and PCBp1 protein expression inversely correlate in patients with breast cancer. (A) Spearman's rank correlation test demonstrated the inverse correlation between PCBp1 protein expression and *miR-490-3p* expression in 10 patients with DCIS (red dots) and 10 patients with IDC (black dots) ($P < 0.05$, Spearman's correlation coefficient-0.801). (B) Representative immunohistochemistry showing PCBp1 expression in breast cancer tissues from DCIS and IDC cases (2 each). DCIS, ductal carcinoma *in situ*; IDC, invasive ductal carcinoma.

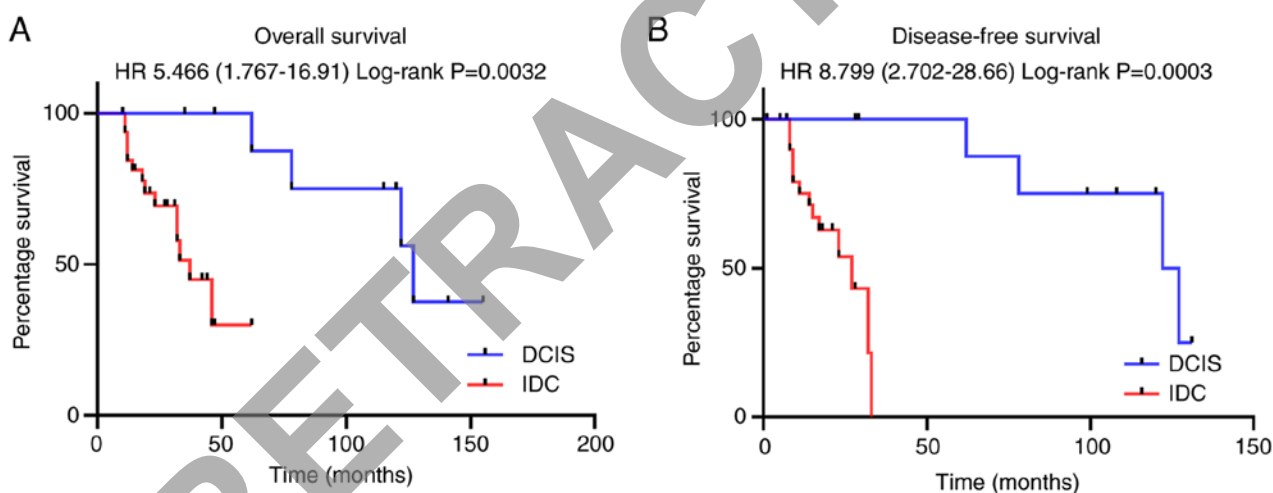


Figure 7. *miR-490-3p* expression is associated with a poor overall survival and prognosis. (A) Kaplan-Meier overall survival analysis curve showed significant lower overall survival in patients with IDC (n=35), who had a higher *miR-490-3p* expression, compared to patients with DCIS (n=10) with a lower *miR-490-3p* expression; $P=0.0032$. (B) Kaplan-Meier disease-free survival analysis curve revealed a significantly poorer prognosis of patients with IDC compared to patients with DCIS; $P=0.0003$. DCIS, ductal carcinoma *in situ*; IDC, invasive ductal carcinoma.

regulatory process or co-occurs with the kinase mediated regulation of RNA binding capacity of PCBp1.

Given the different targets of *miR-490-3p* identified in isolated studies, it would be of utmost importance to perform a genome-wide analysis of mRNA targets of *miR-490-3p* and identify whether they are coordinately regulated. The identification of such a mechanism may pave the way for *miR-490-3p*-based therapeutic intervention for different cancer types, including breast cancer. Based on the results of the present study, it would also be interesting to verify *miR-490-3p* expression in a larger cohort of breast cancer patients at different stages of disease progression. Doing so in samples obtained from the same patient at different stage of disease progression will be even more informative. Finally, the impact of current therapeutic interventions on the expression of *miR-490-3p* and

whether these changes are associated with the chemoresistance observed in breast cancer patients also needs to be determined. It is highly likely that *miR-490-3p* expression plays an important role in chemoresistance, given its observed role in EMT and metastatic progression, processes comprehensively connected to chemoresistance (27,28,39), in the present study.

Acknowledgements

Not applicable.

Funding

The present study was supported by the Tianjin University Science and Technology Development Fund (grant no. 20140116)

and the National Natural Science Foundation of China (No. 81572418).

Availability of data and materials

All data generated or analyzed during the current study are included in this published article or in the associated supplementary files.

Authors' contributions

NL, LL, YZL and MZ performed the experiments. HHZ and XDL analyzed the data. All authors read and approved the final manuscript.

Ethics approval and consent to participate

All experiments involving human samples were conducted in accordance with the protocol approved by the Institutional Review Board of the Tianjin Medical University Cancer Institute and Hospital. Informed consent was obtained from all participants. All animal experiments were approved by the Institutional Animal Care and Use Committee of the Tianjin Medical University Cancer Institute and Hospital.

Patient consent for publication

Not applicable.

Competing interests

The authors declare that they have no competing interests.

References

- Jemal A, Bray F, Center MM, Ferlay J, Ward E and Forman D: Global cancer statistics. CA Cancer J Clin 61: 69-90, 2011.
- Li J, Zhang BN, Fan JH, Pang Y, Zhang P, Wang SL, Zheng S, Zhang B, Yang HJ, Xie XM, et al: A nation-wide multicenter 10-year (1999-2008) retrospective clinical epidemiological study of female breast cancer in China. BMC Cancer 11: 364, 2011.
- Sporn MB: The war on cancer. Lancet 347: 1377-1381, 1996.
- Early Breast Cancer Trialists' Collaborative Group (EBCTCG): Effects of chemotherapy and hormonal therapy for early breast cancer on recurrence and 15-year survival: An overview of the randomised trials. Lancet 365: 1687-1717, 2005.
- Sayer HG, Kath R, Kliche KO and Höffken K: Premenopausal breast cancer: Chemotherapy and endocrine therapy. Drugs 62: 2025-2038, 2002.
- de Bono JS, Tolcher AW and Rowinsky EK: The future of cytotoxic therapy: Selective cytotoxicity based on biology is the key. Breast Cancer Res 5: 154-159, 2003.
- Hu S, Wilson KD, Ghosh Z, Wang Y, Lan F, Ransohoff KJ, Burridge P and Wu JC: MicroRNA-302 increases reprogramming efficiency via repression of NR2F2. Stem Cells 31: 259-268, 2013.
- Card DA, Hebbar PB, Li L, Trotter KW, Komatsu Y, Mishina Y and Archer TK: Oct4/Sox2-regulated miR-302 targets cyclin D1 in human embryonic stem cells. Mol Cell Biol 28: 6426-6438, 2008.
- Liu X, He B, Xu T, Pan Y, Hu X, Chen X and Wang S: MiR-490-3p functions as a tumor suppressor by inhibiting oncogene VDAC1 expression in colorectal cancer. J Cancer 9: 1218-1230, 2018.
- Chen K, Zeng J, Tang K, Xiao H, Hu J, Huang C, Yao W, Yu G, Xiao W, Guan W, et al: miR-490-5p suppresses tumour growth in renal cell carcinoma through targeting PIK3CA. Biol Cell 108: 41-50, 2016.
- Chen S, Chen X, Xiu YL, Sun KX and Zhao Y: MicroRNA-490-3p targets CDK1 and inhibits ovarian epithelial carcinoma tumorigenesis and progression. Cancer Lett 362: 122-130, 2015.
- Lan G, Yang L, Xie X, Peng L and Wang Y: MicroRNA-490-5p is a novel tumor suppressor targeting c-FOS in human bladder cancer. Arch Med Sci 11: 561-569, 2015.
- Li S, Xu X, Xu X, Hu Z, Wu J, Zhu Y, Chen H, Mao Y, Lin Y, Luo J, et al: MicroRNA-490-5p inhibits proliferation of bladder cancer by targeting c-Fos. Biochem Biophys Res Commun 441: 976-981, 2013.
- Zhang LY, Liu M, Li X and Tang H: miR-490-3p modulates cell growth and epithelial to mesenchymal transition of hepatocellular carcinoma cells by targeting endoplasmic reticulum-Golgi intermediate compartment protein 3 (ERGIC3). J Biol Chem 288: 4035-4047, 2013.
- Ou Y, He J and Liu Y: MiR-490-3p inhibits autophagy via targeting ATG7 in hepatocellular carcinoma. IUBMB Life 70: 468-478, 2018.
- Li J, Feng Q, Wei X and Yu Y: MicroRNA-490 regulates lung cancer metastasis by targeting poly r(C)-binding protein 1. Tumour Biol 37: 15221-15228, 2016.
- Gu H, Yang T, Fu S, Chen X, Guo L and Ni Y: MicroRNA-490-3p inhibits proliferation of A549 lung cancer cells by targeting CCND1. Biochem Biophys Res Commun 444: 104-108, 2014.
- Zhao L and Zheng XY: MicroRNA-490 inhibits tumorigenesis and progression in breast cancer. Onco Targets Ther 9: 4505-4516, 2016.
- Zientek-Targosz H, Kunnev D, Hawthorn L, Venkov M, Matsui S, Cheney RT and Ionov Y: Transformation of MCF-10A cells by random mutagenesis with frameshift mutagen ICR191: A model for identifying candidate breast-tumor suppressors. Mol Cancer 7: 51, 2008.
- Cailleau R, Olivé M and Cruciger QV: Long-term human breast carcinoma cell lines of metastatic origin: Preliminary characterization. In Vitro 14: 911-915, 1978.
- Brüner N, Boysen B, Rømer J and Spang-Thomsen M: The nude mouse as an in vivo model for human breast cancer invasion and metastasis. Breast Cancer Res Treat 24: 257-264, 1993.
- Livak KJ and Schmittgen TD: Analysis of relative gene expression data using real-time quantitative PCR and the 2^{-Delta Delta C(T)} method. Methods 25: 402-408, 2001.
- Chaudhury A, Hussey GS, Ray PS, Jin G, Fox PL and Howe PH: TGF-beta-mediated phosphorylation of hnRNP E1 induces EMT via transcript-selective translational induction of Dab2 and ILEI. Nat Cell Biol 12: 286-293, 2010.
- Hussey GS, Chaudhury A, Dawson AE, Lindner DJ, Knudsen CR, Wilce MC, Merrick WC and Howe PH: Identification of an mRNP complex regulating tumorigenesis at the translational elongation step. Mol Cell 41: 419-431, 2011.
- Gao J, Aksoy BA, Dogrusoz U, Dresdner G, Gross B, Sumer SO, Sun Y, Jacobsen A, Sinha R, Larsson E, et al: Integrative analysis of complex cancer genomics and clinical profiles using the cBio-Portal. Sci Signal 6: pl1, 2013.
- Unberath P, Knell C, Prokosc HU and Christoph J: Developing new analysis functions for a translational research platform: Extending the cBioPortal for cancer genomics. Stud Health Technol Inform 258: 46-50, 2019.
- Pastushenko I and Blanpain C: EMT transition states during tumor progression and metastasis. Trends Cell Biol 29: 212-226, 2019.
- Wu HT, Zhong HT, Li GW, Shen JX, Ye QQ, Zhang ML and Liu J: Oncogenic functions of the EMT-related transcription factor ZEB1 in breast cancer. J Transl Med 18: 51, 2020.
- Enerly E, Steinfeld I, Kleivi K, Leivonen SK, Aure MR, Russnes HG, Rønneberg JA, Johnsen H, Navon R, Rødland E, et al: miRNA-mRNA integrated analysis reveals roles for miRNAs in primary breast tumors. PLoS One 6: e16915, 2011.
- Zhang ZZ, Shen ZY, Shen YY, Zhao EH, Wang M, Wang CJ, Cao H and Xu J: HOTAIR long noncoding RNA promotes gastric cancer metastasis through suppression of poly r(C)-binding protein (PCBP) 1. Mol Cancer Ther 14: 1162-1170, 2015.
- Zhang HY and Dou KF: PCBP1 is an important mediator of TGF-β-induced epithelial to mesenchymal transition in gall bladder cancer cell line GBC-SD. Mol Biol Rep 41: 5519-5524, 2014.
- Xue X, Wang X, Liu Y, Teng G, Wang Y, Zang X, Wang K, Zhang J, Xu Y, Wang J and Pan L: SchA-p85-FAK complex dictates isoform-specific activation of Akt2 and subsequent PCBP1-mediated post-transcriptional regulation of TGFβ-mediated epithelial to mesenchymal transition in human lung cancer cell line A549. Tumour Biol 35: 7853-7859, 2014.

33. Ghanem LR, Chatterji P and Liebhaber SA: Specific enrichment of the RNA-binding proteins PCBP1 and PCBP2 in chief cells of the murine gastric mucosa. *Gene Expr Patterns* 14: 78-87, 2014.
34. Song Q, Sheng W, Zhang X, Jiao S and Li F: ILEI drives epithelial to mesenchymal transition and metastatic progression in the lung cancer cell line A549. *Tumour Biol* 35: 1377-1382, 2014.
35. Cho SJ, Jung YS and Chen X: Poly (C)-binding protein 1 regulates p63 expression through mRNA stability. *PLoS One* 8: e71724, 2013.
36. Shi Z, Zhang T, Long W, Wang X, Zhang X, Ling X and Ding H: Down-regulation of poly(rC)-binding protein 1 correlates with the malignant transformation of hydatidiform moles. *Int J Gynecol Cancer* 22: 1125-1129, 2012.
37. Lian WX, Yin RH, Kong XZ, Zhang T, Huang XH, Zheng WW, Yang Y, Zhan YQ, Xu WX, Yu M, *et al*: THAP11, a novel binding protein of PCBP1, negatively regulates CD44 alternative splicing and cell invasion in a human hepatoma cell line. *FEBS Lett* 586: 1431-1438, 2012.
38. Wang H, Vardy LA, Tan CP, Loo JM, Guo K, Li J, Lim SG, Zhou J, Chng WJ, Ng SB, *et al*: PCBP1 suppresses the translation of metastasis-associated PRL-3 phosphatase. *Cancer Cell* 18: 52-62, 2010.
39. Scimeca M, Urbano N, Bonfiglio R, Duggento A, Toschi N, Schillaci O and Bonanno E: Novel insights into breast cancer progression and metastasis: A multidisciplinary opportunity to transition from biology to clinical oncology. *Biochim Biophys Acta Rev Cancer* 1872: 138-148, 2019.



This work is licensed under a Creative Commons
Attribution-NonCommercial-NoDerivatives 4.0
International (CC BY-NC-ND 4.0) License.

RETRACTED